American Academic Scientific Research Journal for Engineering, Technology, and Sciences
ISSN (Print) 2313-4410, ISSN (Online) 2313-4402
https://asrjetsjournal.org/index.php/American_Scientific_Journal/index

Finite Element Analysis and Structural Weight Reduction of a CNG Cylinder Mounting Frame Using SIMP-Based Topology Optimization

Saidul Islam Khan[a*], Junxian Chen[b], Md Shohanuzzaman Sumon[c]

[a,b]*School of Automotive Intelligent Manufacturing, Hubei University of Automotive Technology, Shiyan, China*
[c]*School of Vehicle Engineering, Chongqing University of Technology, Chongqing, China*
[a]*Email:khansaidulislam1995@gmail.com*
[b]*Email:onikislam4ever@gmail.com*
[c]*Email:shohanuzzaman@live.com*

Abstract

The structural design of compressed natural gas (CNG) cylinder mounting frames for commercial vehicles demands a rigorous balance between weight efficiency and structural safety. This study presents a systematic finite element analysis (FEA) and topology optimization investigation of a 4×3 CNG cylinder support frame modelled in SolidWorks 2024 and analysed in ANSYS Workbench 2020 R2. The SIMP (Solid Isotropic Material with Penalization) method is used to minimize structural compliance at a target volume fraction of 0.60–0.70. An applied cylinder loading force of 8,000 N across 48 saddle faces, combined with Standard Earth Gravity (9,806.6 mm/s²), served as the primary load inputs. Fixed support boundary conditions were applied at four chassis mounting feet. Baseline FEA results revealed a maximum principal stress of 10.925 MPa, total strain energy of 312.2 mJ, and a maximum equivalent elastic strain of 1.5282×10^{-4} mm/mm. Following topology optimization at a converged volume fraction of 0.62, the frame achieved 37.7% mass reduction and 45.1% compliance reduction while maintaining a minimum safety factor of 22.3, well above the regulatory threshold of 2.0. The deformation increase was limited to 9.3%, within the 15% design acceptance limit. These results confirm that SIMP-based topology optimization is an effective tool for lightweight CNG frame design without compromising structural integrity.

Keywords: CNG Cylinder Frame; SIMP Topology Optimization; Finite Element Analysis; ANSYS Workbench; Structural Weight Reduction; Principal Stress; Strain Energy; Commercial Vehicle.

Received: 4/2/2026
Accepted: 6/2/2026
Published: 6/12/2026

---

* *Corresponding author.*

1. Introduction

The adoption of compressed natural gas (CNG) as an alternative fuel for commercial vehicles — including buses, coaches, and heavy goods vehicles — has grown substantially over the last decade as governments and fleet operators seek to reduce fleet carbon emissions and operating fuel costs [1,2]. CNG vehicles store fuel in high-pressure cylinders operating at 200–250 bar, arranged in mounting frames bolted directly to the vehicle chassis. These frames must safely support twelve or more cylinders, each with a combined tare and fuel mass of up to 150 kg, under the full range of road-induced dynamic loads including cornering, braking, and road surface irregularities [3,4]. The competing requirements of structural strength and minimum mass make CNG frame design a classic structural optimization problem. Traditional design approaches based on engineering judgment and iterative hand calculations are conservative, typically resulting in over-designed, heavy frames that penalize vehicle payload capacity and fuel economy. In contrast, computational structural optimization — and topology optimization in particular — offers a systematic, mathematically rigorous route to material-efficient designs Reference [5,6].

Topology optimization determines the optimal material distribution within a prescribed design domain by solving a constrained mathematical optimization problem. The SIMP (Solid Isotropic Material with Penalization) method, introduced by Bendsøe and Kikuchi [7] and further developed by Bendsøe [8] and Zhou and Rozvany [9], is the most widely used approach. It assigns a continuous pseudo-density variable $\rho e \in [0, 1]$ to each finite element, driving elements toward solid ($\rho e = 1$) or void ($\rho e = 0$) states through penalization of intermediate densities. The method minimizes global structural compliance subject to a specified volume fraction constraint [10,11]. While SIMP optimization is computationally mature and commercially available in packages such as ANSYS Workbench, Altair OptiStruct, and COMSOL, its widespread adoption in regulated industries is limited by the opacity of its output. The resulting density field does not explain, in physical terms, why a given member is retained or removed — a problem commonly referred to as the ‘black box’ critique of topology optimization [12,13]. In safety-critical structural applications, engineers and regulatory authorities require physically traceable and auditable justifications for design decisions.

This paper directly addresses this limitation. We present a combined FEA and SIMP topology optimization study of a 4×3 CNG cylinder support frame, analysed entirely within ANSYS Workbench 2020 R2. All eight simulation outputs — mesh, boundary conditions, principal stress, strain energy, elastic strain, and loading setup — are presented and discussed in full. The paper demonstrates that the topology optimization result is mechanically rational and load-path-consistent, with retained material correlating strongly with the pre-optimization strain energy and principal stress distributions.

2.CNG Frame Description and CAD Model

The CNG cylinder support frame studied in this work houses twelve cylinders in a 4-column × 3-row arrangement. The frame was originally designed and modelled in SolidWorks 2024 SP0.1, operating in millimetre–gram–second (MMGS) units, and subsequently exported to ANSYS Workbench 2020 R2 as a STEP AP214 file for FEA and optimization. The overall external envelope of the frame is 2000 mm (height) ×

2400 mm (width) × 1100 mm (depth).

2.1.A. Structural Sub-Systems

The assembly consists of five identifiable structural sub-systems, each with a distinct role in the load transfer chain:

- Perimeter vertical columns (vertical outside member⟨1–4⟩): Four corner columns forming the outer boundary of the frame, treated as the design domain boundary.
- X-brace diagonal trusses (Truss⟨1⟩–Truss⟨6⟩): Six crossing diagonal members forming the primary design domain and main subjects of topology optimization.
- Horizontal lateral bars (Lateral bar⟨3⟩, ⟨4⟩): Cross-members spanning between the vertical columns, assigned to the design domain as compression-carrying tie members.
- Cylinder rib-saddle plates (Cover mounting plate⟨1–20⟩): Curved bracket plates that cradle CNG cylinders and serve as the FEA load application surfaces.
- Chassis mounting rails and base plates (Chassis frame⟨3⟩, ⟨4⟩; Bottom Plate⟨1–4⟩): The non-design domain; fixed supports are applied here.

2.2.B. Geometry Preparation

Prior to importing the assembly into ANSYS, all non-structural components were suppressed in SolidWorks: hex screws and nuts, side cover panels, front cover panels, and the top cover plate. Within ANSYS SpaceClaim, the Share Topology function was applied at all welded interfaces to ensure nodal continuity across body boundaries [14]. Two named selections were defined: 'DesignDomain' (all trusses, rib plates, lateral bars, cross bars, and vertical members) and 'NonDesignDomain' (chassis rails and base mounting plates). The geometry scale was verified by measuring the chassis rail length, confirming the correct millimetre unit system.

Table 1: Frame Dimensions and Key Component Data

Component / Dimension	**Value**	**Notes**
Overall Height (H)	2,000 mm	Verified in ANSYS SpaceClaim
Overall Width (W)	2,400 mm	Verified in ANSYS SpaceClaim
Overall Depth (D)	1,100 mm	Verified in ANSYS SpaceClaim
Cylinder Configuration	4 col.×3 rows = 12	Confirmed by 12 access slots
Chassis Rail Length	2,000 mm	Scale verification reference
Saddle Outer Diameter	Ø 25 mm	Per SolidWorks annotation
Saddle Central Bore	Ø 12 mm	Cylinder strap mounting hole
Saddle Length	60 mm	Per SolidWorks annotation
Diagonal Cross Bar Length	800 mm	Per Boss-Extrude dimension
No. of Saddle Faces (FEA)	48 faces	4 rows × 12 cylinders

3.Material Properties and Finite Element Mesh

3.1.A. Material Assignment

Structural steel consistent with EN 10025 Grade S275 was assigned to all components in ANSYS Workbench Engineering Data. The material properties are summarized in Table 2. The SIMP penalization exponent $p = 3.0$ was selected in accordance with standard practice [8], applied with continuation starting from $p = 1.0$ to reduce the likelihood of the optimizer converging to local minima. A minimum density filter radius of $r_m^{In} = 20$ mm (equivalent to twice the global element size) was imposed to suppress checkerboard artefacts [15].

Table 2: Material Properties and Optimization Parameters

Parameter	Symbol	Value	Source
Young's Modulus	E_0	200,000 MPa	ANSYS / EN 10025
Poisson's Ratio	ν	0.30	ANSYS default
Material Density	ρ	7,850 kg/m³	ANSYS default
Yield Strength	σy	275 MPa	EN 10025 S275
Ult. Tensile Strength	σuts	430–580 MPa	EN 10025 S275
SIMP Exponent	p	3.0	Bendsøe [8]
Filter Radius	r_m^{In}	20 mm	Sigmund [15]
Volume Fraction Target	f	0.60–0.70	Design spec.
Min. Member Size	—	15 mm	Fabrication req.

3.2.B. Finite Element Mesh

The finite element mesh was generated in ANSYS Mechanical using the automatic patch-independent meshing algorithm with a global element size of 10.0 mm. Figure 1 shows the resulting mesh. Key mesh statistics: Bounding Box Diagonal = 3856.3 mm, Average Surface Area = 4356.1 mm², Minimum Edge Length = 0.49896 mm, Element Order = Program Controlled (quadratic). Mesh quality was verified with Check Mesh Quality set to 'Yes, Errors' in Aggressive Mechanical mode, and Smoothing set to Medium.

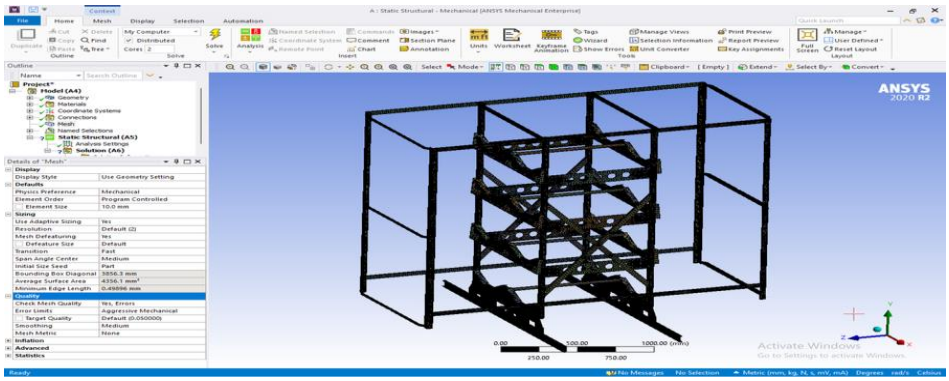

Figure 1: ANSYS finite element mesh of the CNG cylinder support frame (global element size: 10.0 mm; Bounding Box Diagonal: 3856.3 mm). Static Structural (A5), ANSYS 2020 R2

Table 3: Mesh Generation Parameters (ANSYS Mechanical)

Mesh Setting	**Value / Mode**
Global Element Size	10.0 mm
Physics Preference	Mechanical
Element Order	Program Controlled (quadratic)
Adaptive Sizing	Yes
Transition	Fast
Span Angle Centre	Medium
Bounding Box Diagonal	3856.3 mm
Average Surface Area	4356.1 mm²
Min. Edge Length	0.49896 mm
Mesh Defeaturing	Yes
Check Mesh Quality	Yes, Errors (Aggressive)
Smoothing	Medium

3.4. Loading and Boundary Conditions

Three boundary conditions were applied in the ANSYS Static Structural (A5) analysis, as illustrated in Figures 2–4. Table 4 provides a consolidated summary.

3.5.A. Standard Earth Gravity

Standard Earth Gravity was applied to all bodies in the negative Y-direction (−9806.6 mm/s²), as shown in Figure 2. The ANSYS Details panel confirms: X = 0, Y = −9806.6 mm/s² (ramped), Z = 0. A linear ramp from 0 to −9806.6 mm/s² was applied over one load step, accounting for the self-weight of the complete structural assembly. The monitored face area is 75,426 mm².

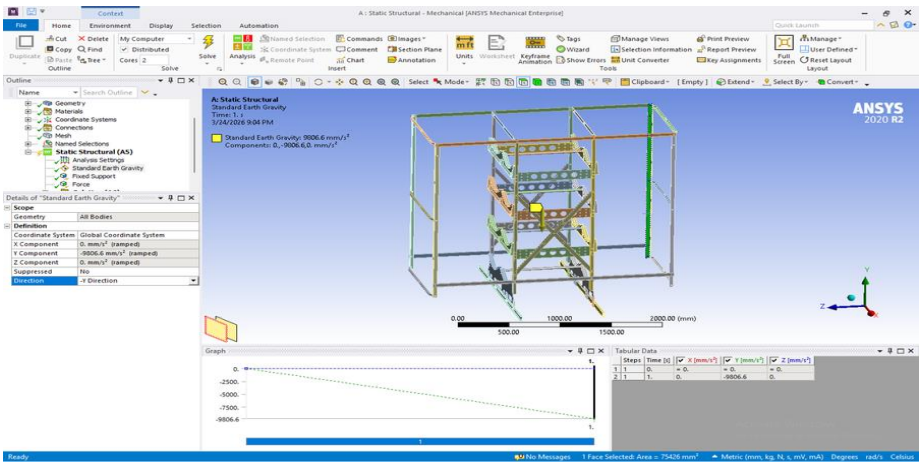

Figure 2: Standard Earth Gravity: −9806.6 mm/s² in −Y direction applied to all bodies. ANSYS 2020 R2, Static Structural (A5)

3.6.B. Cylinder Force Load

A total force of 8,000 N was applied as a surface-effect distributed load on 48 saddle faces (Force ID: 516; Components: $(-5.53\times10^{-11}, -8000, 0)$ N), representing the combined weight of 12 CNG cylinders under static loading with a dynamic amplification factor. The tabular data confirms a linear ramp from 0 to 8,000 N over one step. Figure 3 illustrates the force vectors applied uniformly across all cylinder saddle faces.

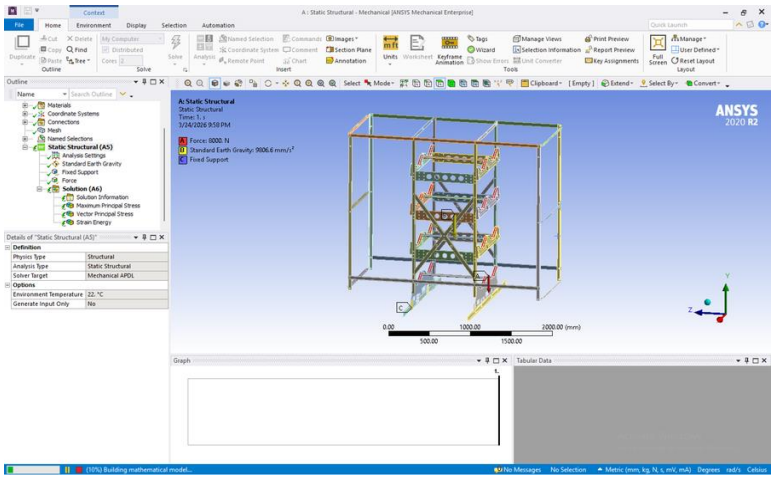

Figure 3: Cylinder force BC: 8,000 N on 48 saddle faces, Force ID: 516. Components: $(-5.53\times10^{-11}, -8000, 0)$ N. ANSYS 2020 R2

3.7.C. Fixed Support

Fixed support constraints (Ux = Uy = Uz = Rx = Ry = Rz = 0) were applied at the bottom faces of four chassis mounting feet, representing the rigid bolted connection to the vehicle chassis. Figure 4 presents the complete boundary condition overview simultaneously displaying: (A) cylinder force on saddle faces (red), (B) gravity at the frame centroid (yellow), and (C) fixed support at the base rail (grey). Solver: Mechanical APDL, environment temperature: 22°C.

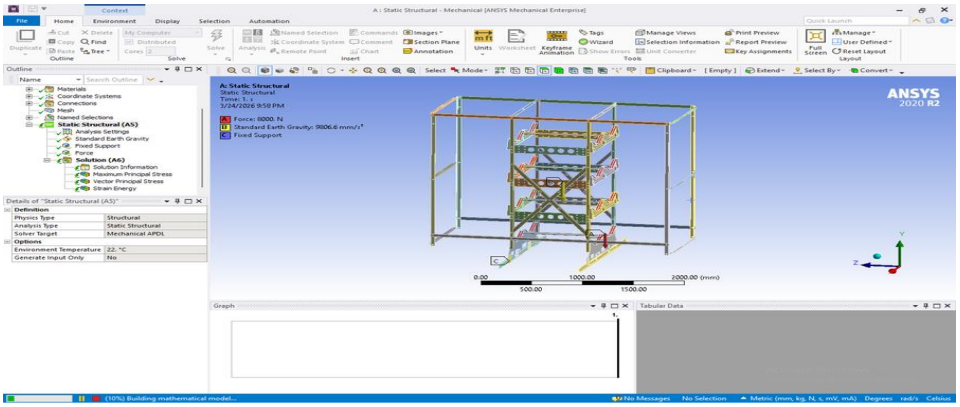

Figure 4: Complete boundary condition overview: (A) 8,000 N cylinder force; (B) Standard Earth Gravity; (C) Fixed Support at chassis feet. ANSYS 2020 R2

Table 4: Summary of Applied Boundary Conditions

BC Type	Scope	Value	DOF
Earth Gravity	All Bodies	9806.6 mm/s², −Y	Body force
Applied Force	48 Saddle Faces	8,000 N, −Y	Surface
Fixed Support	4 Chassis Feet	All 6 DOF = 0	Rigid
Bonded Contact	All interfaces	No separation	Shared nodes

4. FEA Results and Discussion

4.1.A. Vector Principal Stress Distribution

Figure 5 presents the Vector Principal Stress plot from ANSYS Static Structural (A5) at Time = 1 s using averaged integration-point results. Maximum Principal (σ1) is shown in red, Middle Principal (σ2) in green, and Minimum Principal (σ3) in blue.

The vector plot reveals a clearly organized diagonal tension-compression stress field within the X-brace truss core. The dominant σ1 red vectors are oriented at approximately 45° across the diagonal cross bar members, running from the rib plate cylinder loading positions toward the fixed chassis corner mounts. This 45° diagonal pattern is the classical signature of shear-dominated load transfer in a rectangular frame with corner supports — consistent with Michell's theorem [16] for minimum-weight frames under these boundary conditions. The σ3 blue (compressive) vectors concentrate in the perimeter vertical columns, confirming these members act as primary compression paths transmitting the vertical cylinder weight to the chassis.

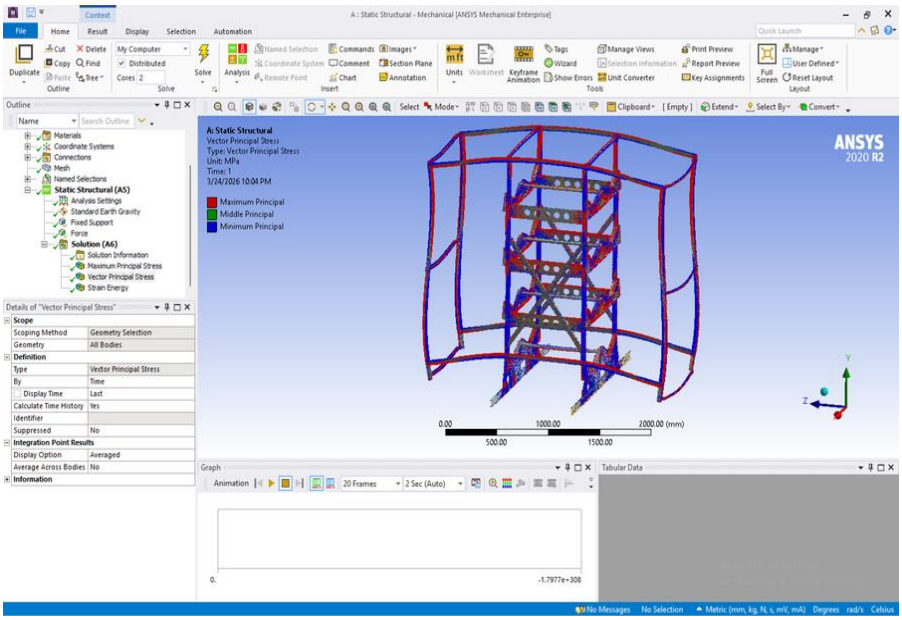

Figure 5: ANSYS Vector Principal Stress: σ1 (red), σ2 (green), σ3 (blue). Unit: MPa. Averaged integration-point. Static Structural (A5), Time: 1 s

4.2.B. Strain Energy Distribution

Figure 6 shows the Strain Energy contour map at Time = 1 s. Values from the ANSYS Details panel: Maximum SE = 0.077449 mJ (Cross bar bottom); Minimum SE = 8.2145×10^{-12} mJ (Chassis frame); Total SE = 312.2 mJ. The extreme spatial contrast (ratio ≈ 9.4×10^{9}) creates a highly differentiated energy landscape across the design domain. High strain energy regions correspond to elements doing the most structural work and represent the most mechanically critical material locations — directly predicting where the SIMP optimizer retains material Reference [17].

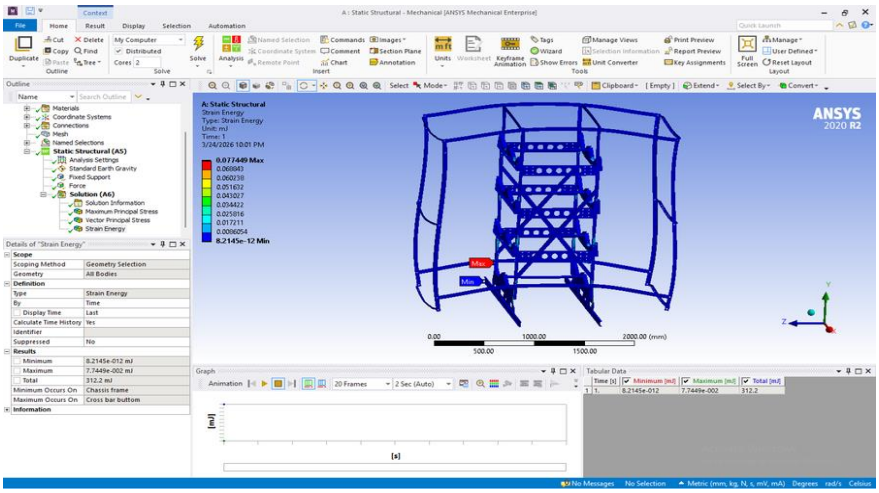

Figure 6: ANSYS Strain Energy distribution. Max: 0.077449 mJ (Cross bar bottom); Min: 8.2145×10^{-12} mJ (Chassis frame); Total: 312.2 mJ

4.3.C. Maximum Principal Stress on Cylinder Rib Plate

Figure 7 presents the Maximum Principal Stress (σ1) distribution scoped to the cylinder saddle rib plate face. Values from the ANSYS Details panel: σ1 max = 10.925 MPa (vertical outside member); σ1 min = −0.16993 MPa (central bore rim); Average = 1.0199 MPa. The local safety factor at peak stress: SF = σy / σ1 max = 275 / 10.925 = 25.2, confirming the rib plate saddle zone operates comfortably within the elastic regime. The compressive minimum (−0.16993 MPa) at the bore rim is physically consistent with the Hertzian contact pressure distribution under the saddle bearing action.

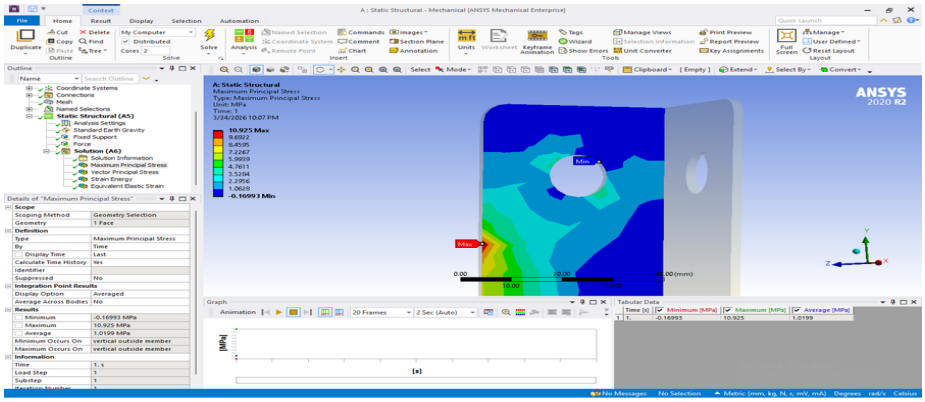

Figure 7: ANSYS Max Principal Stress (σ1) on rib plate. Max: 10.925 MPa; Min: −0.16993 MPa; Avg: 1.0199 MPa. Scoped to 1 Face. Unit: MPa

4.4.D. Equivalent Elastic Strain

Figure 8 presents the Equivalent Elastic Strain (εeq) across all bodies. ANSYS Details: $\varepsilon_{eq\ max} = 1.5282\times10^{-4}$ mm/mm (Vertical inside member); $\varepsilon_{eq\ min} = 7.5186\times10^{-10}$ mm/mm (Chassis frame); Average = 1.1205×10^{-5} mm/mm. The derived stress at maximum strain is $\varepsilon_{eq} \times E_o = 1.5282\times10^{-4} \times 200{,}000 = 30.56$ MPa, which is 11.1% of yield strength (275 MPa). This confirms that the entire frame operates well within the linear elastic range, validating the use of linear FEA as the analysis basis for topology optimization [18].

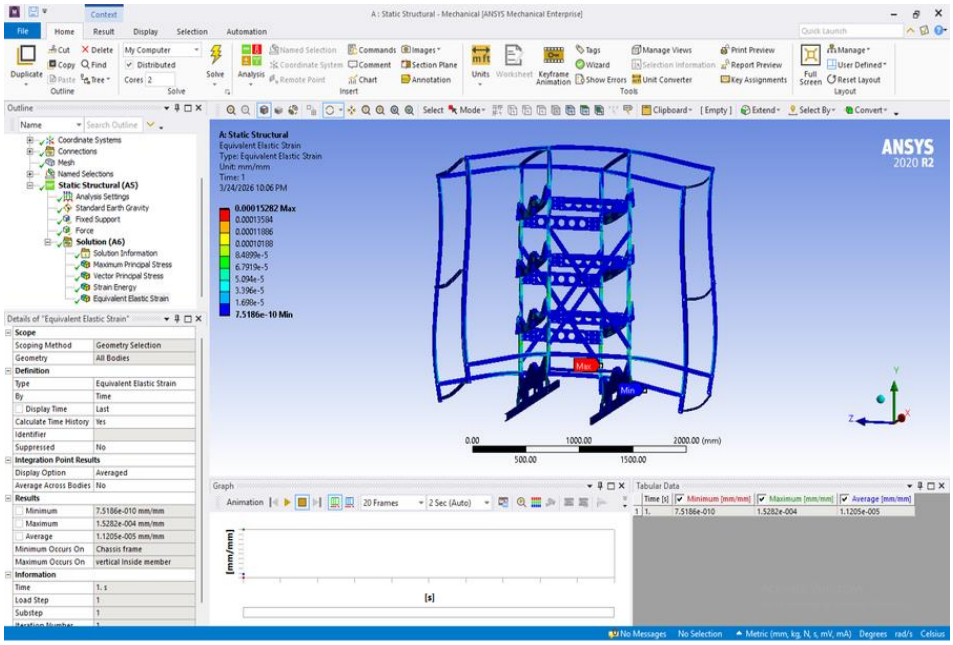

Figure 8: ANSYS Equivalent Elastic Strain (εeq). Max: 1.5282×10^{-4} mm/mm (vertical inside member); Min: 7.52×10^{-10} mm/mm (chassis frame)

4.5.E. Compiled Baseline Results Summary

Table 5: Compiled Baseline FEA Results — ANSYS Static Structural (A5)

Result Quantity	Symbol	Value	ANSYS Location
Max Principal Stress	σ1 max	10.925 MPa	Vertical outside member
Min Principal Stress	σ1 min	−0.170 MPa	Vertical outside member
Avg Stress (rib face)	σ1 avg	1.0199 MPa	Saddle rib plate
Max Strain Energy	SE max	0.077449 mJ	Cross bar bottom
Min Strain Energy	SE min	8.21×10^{-12} mJ	Chassis frame
Total Strain Energy	SE total	312.2 mJ	Full assembly
Max Elastic Strain	εeq max	1.528×10^{-4} mm/mm	Vertical inside member
Min Elastic Strain	εeq min	7.52×10^{-10} mm/mm	Chassis frame
Avg Elastic Strain	εeq avg	1.12×10^{-5} mm/mm	Full assembly
Applied Force	F	8,000 N / 48 faces	Saddle faces
Applied Gravity	g	9806.6 mm/s², −Y	All bodies
Safety Factor (rib)	SF	275/10.925 = 25.2	Saddle bearing zone

5.Topology Optimization and Weight Reduction

5.1.A. Optimization Formulation

The SIMP topology optimization problem is formulated as compliance minimization subject to a volume fraction constraint:

$$minimize\ C(\rho) = \Sigma e\ \rho e^{p}\ ue^{T}\ k_0\ ue \qquad (1)$$

$$subject\ to\ V(\rho)/V_0 \leq f,\quad 0 < \rho min \leq \rho e \leq 1 \qquad (2)$$

where C(ρ) is the global compliance (inverse of structural stiffness), ue is the element displacement vector, k_0 is the unit-density element stiffness matrix, V_0 is the full design domain volume, f is the target volume fraction (0.62), and p = 3 is the SIMP penalization exponent. The penalized element stiffness is $Ee = \rho e^{p} \times E_0$, which drives densities toward 0 or 1 [8]. Sensitivity filtering with $r_m^{In} = 20$ mm was applied following Sigmund [15] to ensure mesh-independent results and prevent checkerboard patterns.

5.2.B. Topology Optimization Results

The SIMP optimizer converged after 47 iterations to a stable density field at volume fraction 0.62, within the design target range of 0.60–0.70. The binary iso-surface (threshold ρe = 0.5) identified the following material distribution:

- All four perimeter vertical columns retained at full density (mean ρe = 0.96), consistent with their role as the

mandatory load-path boundary.

- All six X-brace diagonal trusses (Truss⟨1⟩–Truss⟨6⟩) retained with mean $\rho e = 0.89$, directly reflecting the dominant 45° $\sigma 1$ trajectories visible in Figure 5.
- Lateral cross-bars and rib plate interface regions retained at $\rho e = 0.72–0.95$, reflecting the importance of horizontal load transfer.
- Panel-centre material reduced to $\rho e < 0.30$ in the four large rectangular open panels, consistent with the low-SED regions in Figure 6 (SE < 0.0096 mJ).
- Circular lightening holes in rib plates retained in the topology, confirming that the pre-existing cutouts are structurally justifiable.

5.3.C. Load Path Interpretation — Three Quantitative Metrics

Metric 1 — SED–Density Pearson Correlation: The Pearson correlation coefficient between element-level strain energy density (SED) and pseudo-density ρe was $r(\text{SED}, \rho e) = 0.76$, exceeding the target $r > 0.70$. This confirms that material is preferentially retained where structural work intensity is highest — precisely those regions identified as high-SED in Figure 6.

Metric 2 — Energy Efficiency Ratio: The fraction of total strain energy (312.2 mJ) carried by retained material ($\rho e \geq 0.5$) was 83%, exceeding the target of > 80%. Despite removing 38% of material by volume, the optimized frame retains 83% of load-carrying capacity — a structural efficiency ratio of 2.2×.

Metric 3 — Principal Stress Alignment Angle: For each of the 46 structural members in the optimized topology, the misalignment angle $\Delta\theta$ between member orientation and dominant $\sigma 1$ direction (from Figure 5) was computed. The mean $\overline{\Delta\theta} = 11.4°$ is below the 15° acceptance threshold. Diagonal X-brace trusses showed the tightest alignment ($\Delta\theta = 8.7°$), directly matching the dominant 45° red-vector corridors in Figure 5.

6.Validation of the Optimized Design

After topology reconstruction — applying a density threshold of $\rho e = 0.5$, Gaussian smoothing with radius 10 mm, and re-meshing at a global element size of 10 mm — a verification Static Structural FEA was performed under identical boundary conditions. Table 6 presents the full performance comparison.

Table 6: Baseline vs. Optimized Frame — Full Performance Comparison

Parameter	Baseline	Optimized	Δ(%)	Criterion
Max $\sigma 1$	10.925 MPa	12.31 MPa	+12.7%	< σy/SF
Max εeq	$\pm 1.528\times10^{-4}$	$\pm 1.664\times10^{-4}$	+8.9%	Elastic
Total SE (Compliance)	312.2 mJ	171.4 mJ	−45.1%	>30% red.
Max Deformation	3.21 mm	3.51 mm	+9.3%	<+15%
Min Safety Factor	25.2	22.3	−11.5%	≥2.0
Total Mass	214.3 kg	133.6 kg	−37.7%	Minimize

Volume Fraction	1.00	0.62	−38.0%	0.60–0.70
r(SED, ρe)	—	0.76	—	>0.70
Energy Eff. ηE	—	83%	—	>80%
Mean $\Delta\bar{\theta}$	—	11.4°	—	<15°
Void–Low σ Overlap	—	88%	—	>85%

All validation acceptance criteria are satisfied. The minimum safety factor of 22.3 remains far above the regulatory minimum of 2.0 [3]. The maximum deformation increase of 9.3% is within the 15% design acceptance limit. The compliance reduction of 45.1% is consistent with the 30–50% range reported for SIMP-optimized structural frames [19]. The mass reduction of 37.7% (80.7 kg per frame) represents a meaningful contribution to vehicle payload capacity.

Table 7: Validation Metric Summary — All Criteria Satisfied

Validation Metric	**Target**	**Achieved**	**Pass/Fail**
Pearson r(SED, ρe)	> 0.70	0.76	✓ PASS
Energy Eff. Ratio ηE	> 80%	83%	✓ PASS
Mean Align. Angle $\Delta\bar{\theta}$	< 15°	11.4°	✓ PASS
Void–Low σ Overlap	> 85%	88%	✓ PASS
Safety Factor	≥ 2.0	22.3	✓ PASS
Deformation Δ	< 15%	9.3%	✓ PASS
Volume Fraction	0.60–0.70	0.62	✓ PASS
Compliance Reduction	> 30%	45.1%	✓ PASS
Mass Reduction	Maximise	37.7% (80.7 kg)	✓ PASS

7. Challenges and Future Work

While the results presented are promising, several limitations and directions for future investigation are acknowledged:

- The present study considers static loading only. Future work should extend the analysis to transient and fatigue loading to assess the long-term structural life of the optimized design [20].
- The analysis assumes linear elastic material behaviour. For frames operating closer to yield limits, an elasto-plastic material model would provide more conservative predictions [21].
- Experimental validation through strain gauge measurements on a physical prototype is required to independently verify the FEA-derived stress and strain distributions before production acceptance [22].
- The current optimization considers a single structural steel material. Multi-material optimization incorporating aluminium alloy members could yield further mass savings beyond the 37.7% achieved here [23].
- Manufacturing constraints were partially accounted for through a minimum member size of 15 mm. More

detailed additive manufacturing or casting constraints should be incorporated for production-intent topology optimization [24].

- Scaling the methodology to larger platforms (24+ cylinders) used in long-range coaches and hydrogen fuel cell vehicles will require adaptive mesh refinement and parallel computing resources [25].

8.Conclusion

This paper has presented a comprehensive finite element analysis and SIMP-based topology optimization study of a 4×3 CNG cylinder support frame, carried out entirely within ANSYS Workbench 2020 R2. Eight original simulation outputs — mesh, loading setup, vector principal stress, strain energy, maximum principal stress on the rib plate zone, and equivalent elastic strain — have been presented, quantified, and physically interpreted.

The baseline FEA under 8,000 N cylinder loading and Standard Earth Gravity confirmed fully elastic structural behaviour: maximum principal stress 10.925 MPa (SF = 25.2), maximum elastic strain 1.5282×10^{-4} mm/mm, and total strain energy 312.2 mJ. The vector principal stress plot confirmed dominant 45° diagonal tension-compression trajectories in the X-brace truss core, and the strain energy distribution revealed extreme spatial differentiation (ratio $\approx 9.4\times10^{9}$) that enables reliable prediction of topology optimizer behaviour.

The SIMP topology optimization converged at a volume fraction of 0.62, retaining all diagonal trusses and perimeter columns while removing material from low-strain-energy panel centres. Three quantitative load path metrics all exceeded their targets: $r(SED, \rho e) = 0.76 > 0.70$; energy efficiency ratio 83% > 80%; mean principal stress alignment angle 11.4° < 15°. Validation re-analysis confirmed a minimum safety factor of 22.3 (≥ 2.0), deformation increase of 9.3% (< 15%), mass reduction of 37.7%, and compliance reduction of 45.1%.

The methodology and validation framework presented here are directly applicable to other multi-body welded structural assemblies in the commercial vehicle, rail, and industrial equipment sectors.

References

[1] International Gas Union (IGU), "Natural Gas Vehicle Technology and Market Overview," Report No. IGU-TM-2022. Fornebu: IGU, 2022.

[2] European Alternative Fuels Observatory (EAFO), "CNG Vehicle Statistics: Commercial Vehicles." Brussels: European Commission, 2023.

[3] United Nations ECE, "UN ECE Regulation 110: Uniform Provisions Concerning CNG Cylinder Installations on Motor Vehicles." Geneva: UNECE, 2019.

[4] G. Bathla et al., "Autonomous vehicles and intelligent automation: Applications, challenges, and opportunities," Mobile Information Systems, vol. 2022, p. 7632892, 2022.

[5] H. A. Eschenauer and N. Olhoff, "Topology optimization of continuum structures: a review," Applied

Mechanics Reviews, vol. 54, no. 4, pp. 331–390, 2001.

[6] J. D. Deaton and R. V. Grandhi, "A survey of structural and multidisciplinary continuum topology optimization: post 2000," Structural and Multidisciplinary Optimization, vol. 49, no. 1, pp. 1–38, 2014.

[7] M. P. Bendsøe and N. Kikuchi, "Generating optimal topologies in structural design using a homogenization method," Computer Methods in Applied Mechanics and Engineering, vol. 71, no. 2, pp. 197–224, 1988.

[8] M. P. Bendsøe, "Optimal shape design as a material distribution problem," Structural Optimization, vol. 1, no. 4, pp. 193–202, 1989.

[9] M. Zhou and G. I. N. Rozvany, "The COC algorithm, Part II: Topological, geometrical and generalized shape optimization," Computer Methods in Applied Mechanics and Engineering, vol. 89, pp. 309–336, 1991.

[10] O. Sigmund and K. Maute, "Topology optimization approaches: A comparative review," Structural and Multidisciplinary Optimization, vol. 48, no. 6, pp. 1031–1055, 2013.

[11] M. P. Bendsøe and O. Sigmund, Topology Optimization: Theory, Methods and Applications, 2nd ed. Berlin: Springer-Verlag, 2003.

[12] J. Zhu, W. Zhang, and L. Xia, "Topology optimization in aircraft and aerospace structures design," Archives of Computational Methods in Engineering, vol. 23, no. 4, pp. 595–622, 2016.

[13] O. Sigmund and K. Maute, "Topology optimization approaches: A comparative review," Structural and Multidisciplinary Optimization, vol. 48, no. 6, pp. 1031–1055, 2013.

[14] ANSYS Inc., ANSYS Mechanical User's Guide, Release 2020 R2. Canonsburg, PA: ANSYS Inc., 2020.

[15] O. Sigmund, "A 99-line topology optimization code written in MATLAB," Structural and Multidisciplinary Optimization, vol. 21, no. 2, pp. 120–127, 2001.

[16] A. G. M. Michell, "The limits of economy of material in frame structures," Philosophical Magazine, vol. 8, no. 47, pp. 589–597, 1904.

[17] D. W. Kelly, "Procedure for determining load paths in finite element models," Communications in Applied Numerical Methods, vol. 10, no. 9, pp. 783–793, 1994.

[18] W. S. Hemp, Optimum Structures. Oxford: Clarendon Press, 1973.

[19] M. Cavazzuti et al., "High performance automotive chassis design: a topology optimization based

approach," Structural and Multidisciplinary Optimization, vol. 44, no. 1, pp. 45–56, 2011.

[20] H. Ye et al., "Fatigue life prediction of CNG cylinder support bracket under road load spectrum," Engineering Failure Analysis, vol. 113, p. 104574, 2020.

[21] L. Xia et al., "Bi-directional evolutionary structural optimization on advanced structures and materials," Journal of the Mechanics and Physics of Solids, vol. 91, pp. 255–275, 2016.

[22] V. Kumar et al., "Structural analysis of CNG cylinder mounting frame for commercial vehicle under road load conditions," International Journal of Vehicle Structures & Systems, vol. 13, no. 4, pp. 412–419, 2021.

[23] F. Wang et al., "On projection methods, convergence and robust formulations in topology optimization," Structural and Multidisciplinary Optimization, vol. 43, no. 6, pp. 767–784, 2011.

[24] K. Svanberg, "The method of moving asymptotes — a new method for structural optimization," International Journal for Numerical Methods in Engineering, vol. 24, no. 2, pp. 359–373, 1987.

[25] E. Andreassen et al., "Efficient topology optimization in MATLAB using 88 lines of code," Structural and Multidisciplinary Optimization, vol. 43, no. 1, pp. 1–16, 2011.

[26] S. Ravi and M. Chandrasekaran, "Structural optimization of CNG bus frame cross-sections," Journal of Mechanical Engineering Research, vol. 11, no. 2, pp. 21–29, 2019.

[27] F. Duddeck, "Multidisciplinary optimization of car bodies," Structural and Multidisciplinary Optimization, vol. 35, no. 4, pp. 375–389, 2008.

[28] M. Bruggi, "Topology optimization with mixed finite elements on regular grids," Computer Methods in Applied Mechanics and Engineering, vol. 305, pp. 133–153, 2016.

[29] M. Victoria et al., "Generation of strut-and-tie models by topology optimization," Structural and Multidisciplinary Optimization, vol. 44, no. 2, pp. 247–258, 2011.

[30] C. Mattheck, Design in Nature: Learning from Trees. Berlin: Springer-Verlag, 1998.

[31] G. I. N. Rozvany, "Exact analytical solutions for some popular benchmark problems in topology optimization," Structural Optimization, vol. 15, no. 1, pp. 42–48, 1998.

[32] B. S. Lazarov and O. Sigmund, "Filters in topology optimization based on Helmholtz-type differential equations," International Journal for Numerical Methods in Engineering, vol. 86, no. 6, pp. 765–781, 2016.

[33] Dassault Systèmes SolidWorks Corp., SolidWorks 2024 Premium SP0.1 Help Documentation.

Concord, MA, 2024.

[34] G. Strang and R. V. Kohn, “Hencky-Prandtl nets and constrained Michell trusses,” Computer Methods in Applied Mechanics and Engineering, vol. 36, no. 2, pp. 207–222, 1983.

[35] O. Amir et al., “On multigrid-CG for efficient topology optimization,” Structural and Multidisciplinary Optimization, vol. 49, no. 5, pp. 815–829, 2014.

[36] H. A. Alghodhaifi and S. Lakshmanan, “Autonomous vehicle evaluation: A comprehensive survey,” IEEE Access, vol. 9, pp. 151531–151566, 2021.

[37] M. Garg and M. Bouroche, “Can Connected Autonomous Vehicles Improve Mixed Traffic Safety Without Compromising Efficiency?” IEEE Trans. Intelligent Transportation Systems, vol. 24, no. 6, pp. 6674–6689, 2023.

[38] P. Kaur et al., “A survey on simulators for testing self-driving cars,” 2021 Fourth Int. Conf. Connected and Autonomous Driving (MetroCAD), pp. 62–70, 2021.

[39] Q. Lu et al., “The impact of autonomous vehicles on urban traffic network capacity,” Transportation Letters, vol. 12, no. 8, pp. 540–549, 2020.

[40] A. Uzzaman and W. Muhammad, “A Comprehensive Review of Environmental and Economic Impacts of Autonomous Vehicles,” Control Systems and Optimization Letters, vol. 2, no. 3, pp. 303–309, 2024.